Influence of topographically patterned angled guidelines on directed self-assembly of block copolymers

Nathan Rebello, Vaidyanathan Sethuraman, Gregory Blachut, Christopher J. Ellison, C. Grant Willson, and Venkat Ganesan*
Department of Chemical Engineering, University of Texas at Austin, Austin, Texas 78712, USA
(Received 4 July 2017; published 8 November 2017)

Single chain in mean-field Monte Carlo simulations were employed to study the self-assembly of block copolymers (BCP) in thin films that use trapezoidal guidelines to direct the orientation and alignment of lamellar patterns. The present study explored the influence of sidewall interactions and geometry of the trapezoidal guidelines on the self-assembly of perpendicularly oriented lamellar morphologies. When both the sidewall and the top surface exhibit preferential interactions to the same block of the BCP, trapezoidal guidelines with intermediate taper angles were found to result in less defective perpendicularly orientated morphologies. Similarly, when the sidewall and top surface are preferential to distinct blocks of the BCP, intermediate tapering angles were found to be optimal in promoting defect free structures. Such results are rationalized based on the energetics arising in the formation of perpendicularly oriented lamella on patterned substrates.

DOI: 10.1103/PhysRevE.96.052501

I. INTRODUCTION

In the present era of increasing interest in smaller, faster, and more energy efficient electronic devices that can power modern electronics, directed self-assembly (DSA) of block copolymer (BCP) domains has emerged as a potential tool for enhancing advanced semiconductor local guidelining and disk drive manufacturing techniques [1–8]. The ability of block copolymers to self-assemble at molecular length scales makes them suitable candidates for sub-20-nm scale lithography applications that are needed for the fabrication of device features or elements [5,6]. In this regard, perpendicularly oriented and aligned lamellar structures in thin films have proven especially relevant for such applications [9,10]. However, an ability to achieve such morphologies which are simultaneously defect free remains an outstanding challenge.

To achieve directed self-assembly of block copolymers, self-assembled lamellar and cylindrical morphologies must be induced to orient perpendicular to the substrate. This is usually accomplished by tuning the interaction between the blocks of the copolymers and both the substrate and the air or top coat. A second constraint is that the perpendicularly oriented lamella must be aligned to provide long-range order, and this is accomplished in one of two ways: one method is graphoepitaxy, in which lithographically defined guidelines that are as thick or thicker than the BCP film are set at multiples of a particular pitch [11–15]. Alternatively, in the process termed chemoepitaxy, guidelines are fabricated in the substrate that serve to provide a contrast in surface interactions but otherwise do not serve as topographical constraints [16–18].

While a number of experiments have demonstrated the efficacy of both grapho- and chemoepitaxy for aligning oriented morphologies, recently, we found that a hybrid process, can serve as a more facile approach for achieving such an objective [19]. In the hybrid approach, the guidelines have a finite thickness (but smaller than the film thickness) and have cross sections that can be varied from rectangular to trapezoidal shapes. In contrast to graphoepitaxy, however, the interaction of the polymer components with the sidewalls and the top surface of the guidelines can be modulated, and serves as an additional driving force for alignment. Such a hybrid process is schematically depicted in Fig. 1, wherein the blue domain is rich in monomer A and red domain is rich in monomer B. The composition of the backfilled brush, the dimensions of the guideline, and the strength at which the sidewall and top surface interact with BCP components have all been observed to play an important role on the resulting morphologies of the overlaying BCP and the degree of alignment that is achieved [18].

Inspired by the above advances, in a previous study [20], we used computer simulations to study the effects of film thickness and grafting density on the orientational order achieved in DSA for the case of a *rectangular* geometry of the guideline [Fig. 1(a)]. The efficacy of the epitaxy process is often measured in terms of density multiplication factor (M), which is defined as the ratio of the lateral distance over which defect free alignment is observed to the pitch (X) of the lamellar domain, and experiments typically aim at 2X-8X density multiplication. Using our simulations, we identified conditions for DSA formulated in terms of the range of parameters that facilitate higher extent of density multiplication [20,21].

Recent experiments have shown that the guiding lines fabricated in the above hybrid strategy may not necessarily possess a strictly rectangular topology. Indeed, imperfections arising from process fabrication conditions can themselves lead to defects in the taper angle and width of such guidelines. On the other hand, it has also been shown that by carefully controlling the etch rate and the isotropy of reactive ion etch process [22,23], trapezoidal shapes with controlled taper angles can be achieved [Fig. 1(b)]. Such a fabrication strategy opens up an additional parametric handle, viz., the geometry of the guidelines, as a means to influence the efficacy of the DSA. However, there is still a lack of understanding whether the DSA achieved using such trapezoidal guidelines are indeed better than the rectangular geometries, and moreover, whether there are parametric conditions of taper angle, guideline widths and heights, and substrate interactions which promote optimal (defect-free) alignment and orientation of the overlaying block copolymer film.

*venkat@che.utexas.edu

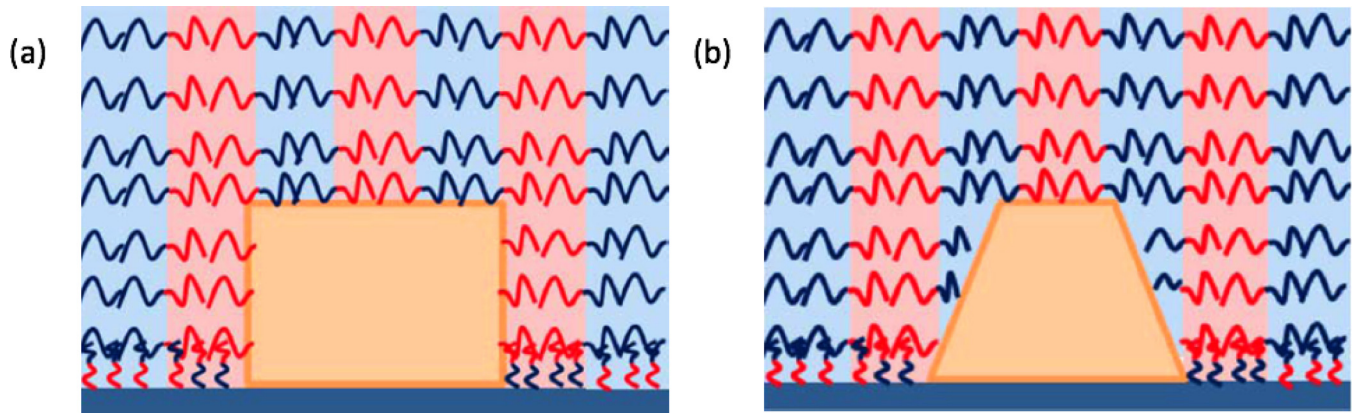

FIG. 1. Schematic of an assembled BCP system to scale with (a) rectangular guideline and (b) trapezoidal (tapered) guideline. Grafted neutral copolymer brushes line substrate (dark blue) between the guideline. By modulating the interaction of the copolymer with the substrate side and top, effective directed self-assembly can be achieved.

Motivated by the above experimental developments, the present work builds on our earlier computer simulation study [20] and focuses on extracting an understanding of the influence of the geometry of the guideline on the efficacy of the DSA epitaxy. For this purpose, we consider the situation of a fixed 4X density multiplication in alignment, and within such a context examine the influence of the guideline width, height, the angle between the guideline sidewall and film bottom, and the interactions between the polymer and the top or sidewalls, in facilitating defect free perpendicular *orientations* of the lamella morphology. The present study does not specifically seek to quantify defects in *alignment* of the morphologies. Instead, we use findings from our previous work [20] and our own preliminary results for the present work (see Sec. III), which demonstrate that: (a) Morphological defects in orientational order are often correlated to defects in long-range alignment; and (b) morphologies which exhibit near perfect alignment from a top view perspective of the film may still exhibit defects in orientation which are undesirable for DSA processes. Hence, we use the quality of perpendicular orientational registry achieved by the morphologies as a computationally feasible measure for identifying the efficacy of the hybrid graphochemoepitaxy in facilitating alignment of perpendicular morphologies.

In this work, the methodology of single chain in mean field simulations was adapted (see Sec. II) to study the influence of a trapezoidal guideline geometry on the self-assembly of BCPs [20]. In Sec. III we present a discussion on our use of a two-dimensional framework for simulations, and the connection between defects in orientational order and the alignment of the morphologies. Subsequently, we consider two model situations for the interactions between the guidelines and the block copolymer components, and in Sec. IV A we present a discussion of the studies underlying the parametric choices for the respective cases. In the first case studied (Sec. IV B), the top surface and sidewall were assumed to be preferential to the same block of the BCP, and in the second case studied (Sec. IV C), the sidewall and top surface were assumed to be preferential to different components. Within these specific parametric spaces, we characterized the influence of the guideline geometry, specifically their taper angle and height on the formation of defect-free perpendicular morphologies. We conclude with a brief summary of our findings.

II. SIMULATION METHODOLOGY

The single chain in mean field (SCMF) simulation approach was employed to model and study the self-assembly of block copolymers in thin films [24–31]. The system was modeled as containing n AB BCP bead-spring chains with $N+1$ beads in each chain. The backfilled brush region was modeled as a random copolymer brush composed of the same A and B segments with $f = 0.5$. Intramolecular bonded interactions $[H_b(\mathbf{r})]$ in both the random copolymer brush and the overlaying block copolymer were treated explicitly using a harmonic spring interaction model [32]:

$$\frac{H_b[\mathbf{r}_i(s)]}{k_BT} = \frac{3}{2b^2}\sum_{i=1}^{n}\sum_{s=1}^{N}[\mathbf{r}_i(s)-\mathbf{r}_i(s+1)]^2, \qquad (1)$$

where $\mathbf{r}_i(s)$ denotes the coordinates of the sth monomer on the ith chain, and b is the bond length between adjacent monomers.

The interactions between the monomers and the guideline hard surface $[H_s(\mathbf{r})]$ were modeled using a short-range potential of the form [15,21,33–35]

$$\frac{H_s(\mathbf{r},K)}{k_BT} = \frac{\Lambda_i^K(x,y)}{d_s}\exp\left(-\frac{z^2}{2d_s^2}\right), \qquad (2)$$

where Λ_i^K (normalized to k_BT) indicates the interaction strength of a monomer at location (x, y) of block K (A or B) with surface i [i = sidewall (SW), film top (FT), top of guideline (ST)], and d_s represents the range of interaction. The relative Λ_i^K of the two blocks represents the degree of favorable and unfavorable interaction with the specified substrate. In Eq. (2), z represents the perpendicular distance between monomer at location (x, y) and the plane of substrate under consideration.

In SCMF, the nonbonded energy interactions are accounted by using psuedopotential fields to model the intermolecular incompatibility (ω) and incompressibility (π) conditions

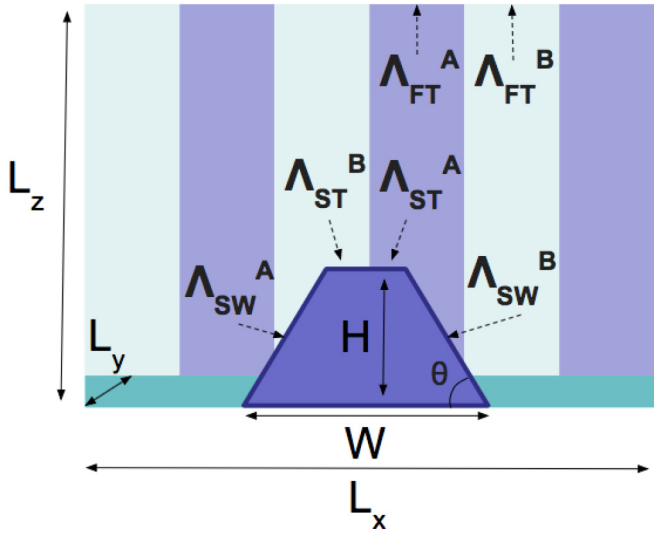

FIG. 2. The following parameters characterize our model: film dimensions (L_x, L_y, L_z), guideline height (H), width (W), taper angle (θ), and the relative chemical affinities of the guideline top surface (ST), thin film top (FT), and sidewall (SW) for each block.

[29,32]:

$$\omega(\mathbf{r}) = \frac{\chi N}{2}[\phi_A(\mathbf{r}) - \phi_B(\mathbf{r})] \tag{3}$$

and

$$\pi(\mathbf{r}) = \frac{\kappa N}{2}[\phi_A(\mathbf{r}) + \phi_B(\mathbf{r}) - 1]. \tag{4}$$

The χ above represents the Flory-Huggins interaction parameter between A and B segments, and κ represents a parameter that embodies the overall (inverse) compressibility of the melt. The quantities $\phi_\alpha(\alpha = \mathrm{A, B})$ represent the instantaneous local volume fractions of α segments, and N denotes the degree of polymerization. We fixed N for BCP at 33 for all the simulations performed in this work. In terms of the above fields, A and B polymer segments at a location $\mathbf{r}$ experience the potentials $-\omega(\mathbf{r}) + \pi(\mathbf{r})$ and $\omega(\mathbf{r}) + \pi(\mathbf{r})$, respectively.

An important quantity that characterizes the system apart from the interaction parameters is the invariant degree of polymerization ($\bar{N}$), which is quantified as the square root of the number of chains per unit volume. For all our simulations, we used $\bar{N} = 110$. The box size parallel to the substrate is fixed at $L_x = 16.24R_g$, which corresponds to a 4X multiplier. We used a grid size of 0.35 R_g. Such a value is chosen close to the statistical segment length ($0.42R_g$) of a homopolymer consisting of the same number of beads as in the BCP.

The SCMF approach was implemented within a Metropolis Monte Carlo framework. In addition to the monomer displacement moves, the simulation used global moves such as chain translation and slithering snake approaches for faster equilibration [36]. Global moves such as chain translation and slithering snake are employed after every 10 steps of monomer displacement moves. After one Monte Carlo (MC) step per particle, potential fields at every location are updated. After 7.5×10^4 MC steps, the final system orientation is analyzed.

A schematic of the different parameters underlying our model are shown in Fig. 2. These include: the width of the bottom surface (W) and the height (H) of the guideline; the taper angle of the guideline θ; six parameters that quantify the interaction affinity between the sidewall of the guidelines, the top surface, and film top with components A and B of the BCP. Figure 3 displays a simplified schematic when the guideline is absent.

To identify the efficacy of the DSA facilitated by the guidelines, a series of cases were considered with different parameters corresponding to the guideline height (H), bottom width (W), and the taper angle θ. Since absolute free energies cannot be easily discerned in SCMF, different initial samples of random configuration of the BCP and grafted copolymers in space were utilized to probe the final morphology (for every parametric condition, at least five different initial configurations were used). The "quality" of the resulting perpendicular lamellar orientation was represented by a "score" that quantified the interfacial area [37] between A and B phases observed for the specific parametric conditions relative to the value expected for a perfectly oriented perpendicular lamella for 4X ($L_x = R_g$) density multiplication. In this representation, the maximum score of unity corresponds to a perfectly oriented morphology, and a lower score indicates a greater degree of defects in vertical orientation. The score is computed as

$$\mathrm{Score} = \frac{3n_i\left(\frac{L_z}{\delta z} - \frac{H}{\delta z} - 1\right) + 3\left(\frac{H}{\delta z} - 1\right)\left(n_i - n_i^t\right) + 2\left(n_i - n_i^t\right) + 2n_i}{n_{\mathrm{AB}}}, \tag{5}$$

where n_i, δz, and n_i^t represent the total number of interfaces, grid spacing in Z direction and the number of interfaces above the top surface respectively. n_{AB} represents the number of AB interfaces from simulation. To identify an interface, we compute the density of A and B particles in each grid and each grid is assigned as A or B depending upon which density is higher in that given cell. An interface is defined as those wherein the A has B neighbors or vice-versa. For perfectly aligned lamellar the score (Score) equals unity. Any deviation from perfectly aligned lamellar generated more AB interfaces, thus leading to a value lesser than 1. Some illustrative morphologies and their scores are presented in Fig. 4.

III. ORIENTATION VERSUS ALIGNMENT

In this work, we sought to quantify the defects (and scores) based on the influence of the guidelines on the perpendicular *orientation* of the morphology rather than on the long length scale *alignment* of the morphologies themselves. Such a framework enables us to use a computationally efficient

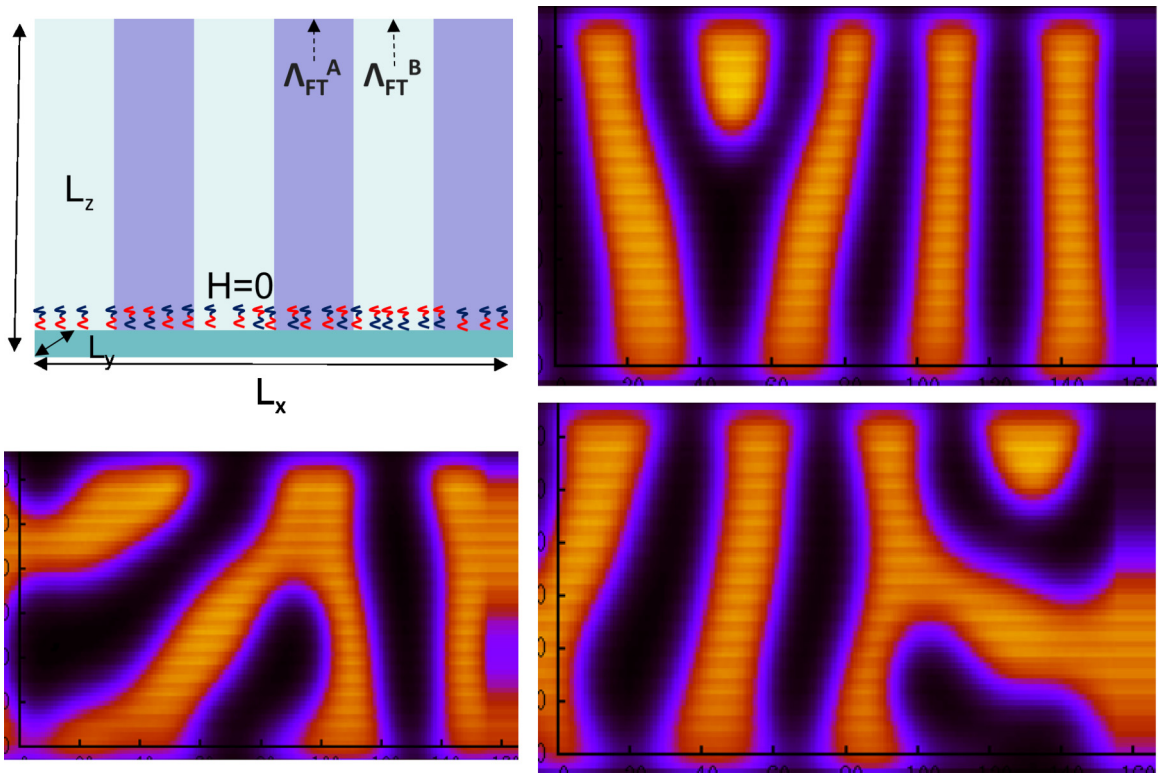

FIG. 3. Displayed is a simplified schematic for a model without a guideline along with 2D maps of sample configurations with different Λ_{FT}^{A} and Λ_{FT}^{B} initial conditions. Only the interaction parameters Λ_{FT}^{A} and Λ_{FT}^{B} play a role in BCP self assembly when the guideline is absent.

approach in which the potential fields of Eqs. (3) and (4) can be evolved in two dimensions, and moreover, an averaging over the transverse direction of the film (Z) can be effected to improve the statistics and reduce the effects of fluctuations. Nevertheless, we undertook preliminary investigations to probe the correlation, if any, between the occurrence of defects in orientation and the alignment characteristics. For such investigations, we considered a few randomly selected

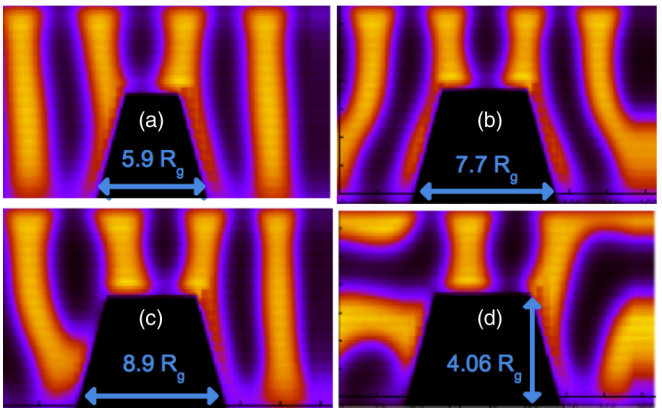

FIG. 4. Two dimensional cross section of the density of A segments with varying bottom guideline widths (W) [(a)–(c)], but possessing the same height ([$H = 4.06R_g$ ($1.0L_o$)]. (c) and (d) have the same geometry but different interaction affinities. The scores for the different morphologies are as follows: (a) 0.95, (b) 0.84, (c) 0.88, and (d) < 0.75.

parameters and effected three-dimensional simulations which capture both the alignment and orientational characteristics of the morphologies, and compared the results with two dimensional transversely averaged simulations for the same parameters. The latter captures only the orientational characteristics of the morphologies, and implicitly assumes that the morphologies exhibit perfect alignment in the transverse direction. The results of such comparisons are summarized below.

Figure 5 displays representative morphologies (corresponding to the density map of A segments) in two-dimensional (2D) and three-dimensional (3D) simulations configurations with the same guideline geometries, film dimensions, and energetic interaction parameters. As seen therein, and based on a number of such representative 3D simulations (not displayed), we were able to deduce the following general findings:

(1) Morphologies that exhibit near-perfect *alignment* (from a top-view perspective) may not always yield near-perfectly *oriented* perpendicular lamella [Fig. 5(a)]. We note that recent work by the groups of Nealey, de Pablo, and coworkers [38] have come to similar conclusions by three-dimensional characterization of their experimental morphologies;

(2) In general, defects observed in the orientation of lamellae in 2D simulations also manifest as defects in long-range alignment in 3D simulations [Fig. 5(b)];

(3) For specified parameters, there is a direct correlation between the morphological scores (as defined in the preceding section) deduced through the 2D and 3D simulations [Figs. 5(a)–5(c)].

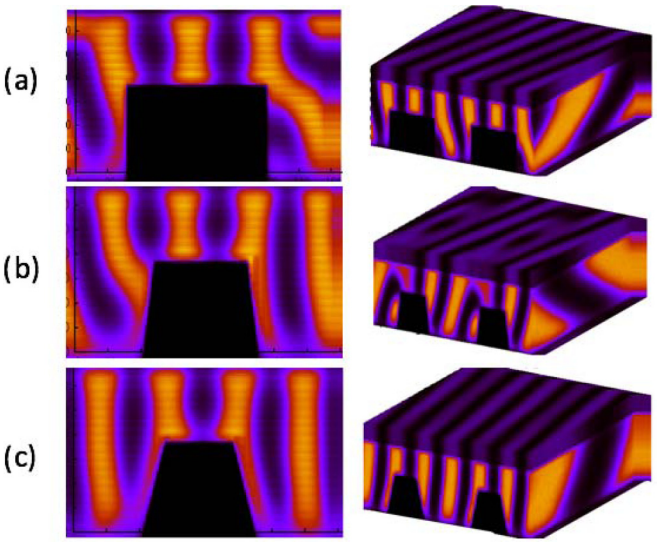

FIG. 5. Representative morphologies (corresponding to the volume fraction profiles of A segments) from 2D and 3D simulations. The respective scores are: (a) 0.81 (2D) and 0.78 (3D); (b) 0.86 (2D) and 0.75 (3D); (c) 0.96 (2D) and 0.94 (3D).

While the above results are based on a limited set of parameters, nevertheless, such findings suggest that quantifying the influence of guideline geometries and energetic parameters on defects in perpendicular orientation of lamella may serve as an indirect approach to identify the influence of guideline parameters on the alignment of the block copolymer assemblies. Based on such considerations, in the following sections we restrict our discussion to the influence of the guidelines on the perpendicular *orientation* of the morphology.

IV. RESULTS AND DISCUSSION

The model adopted in this present work is characterized by a vast parameter space which renders any systematic investigation a challenge. To bring a rational approach to our investigations, we started with a representative geometry for the guidelines and identified the specific interaction characteristics of the A, B components with the top of the film and the top or sidewalls of the guideline, to facilitate optimal perpendicular alignment. Using the representative parametric choices gleaned from such investigations, we probed the effect of χN to identify its influence on the orientational order. Subsequently, we localized our studies to fixed choices of the Flory-Huggins parameter and surface interactions and quantified the influence of the geometrical characteristics of the guidelines upon the orientation of the lamellae. In Sec. IV A we first discuss in brief the studies that we undertook to narrow the choice of energetic parameters used for quantifying the influence of guideline geometry.

In the subsequent sections, we describe our results categorized based on the qualitative characteristics of the surface energies between the sidewall or top surface of the guidelines and the respective polymer components. In the first set of results (Sec. IV B), both the sidewall and top surface were assumed to be preferential to component A. In the second set of results (Sec. IV C), the top surface was assumed to be preferential to component A, whereas the sidewall was assumed to exhibit favorable interactions with component B. For both sets of simulations, a range of guideline (bottom) widths, heights, and taper angles were examined (we report our results in terms of widths normalized by the lamellar width $L_o = 4.06R_g$) [20].

A. Choice of parametric conditions

For the model depicted pictorially in Fig. 2, it can be observed that six independent guideline and film interaction parameters, viz., $\Lambda^A_{\rm FT}, \Lambda^B_{\rm FT}, \Lambda^A_{\rm ST}, \Lambda^B_{\rm ST}, \Lambda^A_{\rm SW}, \Lambda^B_{\rm SW}$ (all energies below are reported in k_BT units), need to be chosen before studying the effect of the guideline geometry on the lamellae orientation. Guided by physical and experimental considerations, we conducted a series of initial studies to identify the range of energetic interaction parameters (between the A and B components with the top of the film, and top or sidewalls of the guidelines) which facilitate perpendicular lamella orientations.

For reference, we studied the case where there is no guideline ($W = 0$) [39]. Such a system resulted in a score of 0.805. For the rest of the manuscript, we consider the influence of the guideline geometrical parameters upon the scores of morphology. To isolate the influence of the guidelines, we considered a situation where the top interface of the confined block copolymer film is "neutral" to both A and B segments of the copolymer [22] and set $\Lambda^A_{\rm FT} = \Lambda^B_{\rm FT} = 1.6$. Further, the choice of the interaction parameters with the sidewall and the top of guidelines were informed by the reasoning that strongly favorable polymer-guideline interactions (i.e., large $\Lambda^i_{\rm ST}$ or $\Lambda^i_{\rm SW}$) will result in conditions where the energetics of such interactions dominate all the other geometric and energetic effects in the system. Similarly, very weak polymer-guideline interactions (small $\Lambda^i_{\rm ST}$ or $\Lambda^i_{\rm SW}$) are expected to render the influence of guidelines and its geometry irrelevant in influencing the orientation of the lamella. Through a number of parametric studies guided by the preceding ideas, it was determined that the sidewall interaction parameters ($\Lambda^i_{\rm SW}$) in the range of 1.5–6.5 allowed for tangible influence of the guideline geometry while not simultaneously overwhelming all other effects. Based on such results, we set $\Lambda^A_{\rm SW}$ to 4.0 and $\Lambda^B_{\rm SW}$ to 6.0, corresponding to the conditions where the sidewall of the guideline is preferentially attracted to the component A.

For the results presented in Sec. IV B, as a final step, we probed the influence of the interactions between the top of the guideline and the A, B components ($\Lambda^A_{\rm ST}$ and $\Lambda^B_{\rm ST}$). It was found for the case where both the guideline top and sidewall attract the same component of the BCP (in our notation, the A segments), maximum scores are obtained when there exists only a weak disparity between $\Lambda^A_{\rm ST}$ and $\Lambda^B_{\rm ST}$, as revealed in Fig. 6. Representative morphologies for such a case are displayed in Figs. 7(a) and 7(b), in which it can be observed that when there is a large disparity between the $\Lambda^A_{\rm ST}$ and $\Lambda^B_{\rm ST}$ [Fig. 7(a)], a small "film" of A monomers form on the top surface of the guideline. In contrast, morphologies with less defective perpendicular orientation are observed when there exists a weak disparity between $\Lambda^A_{\rm ST}$ and $\Lambda^B_{\rm ST}$ [Fig. 7(b)]. Based on such results, we chose $\Lambda^A_{\rm ST} = 0$ and $\Lambda^B_{\rm ST} = 1$.

The results presented in Sec. IV C correspond to the case where the top and sidewalls of the guideline are preferential to

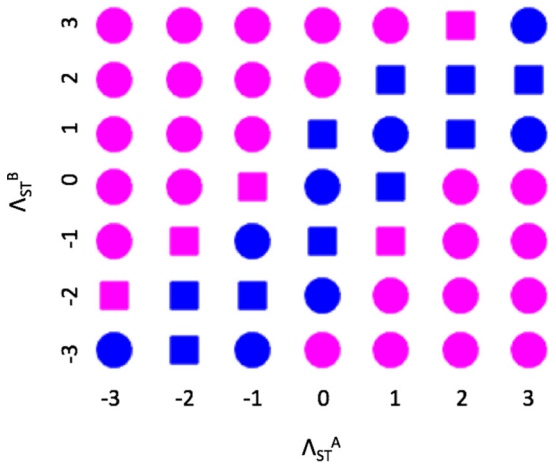

FIG. 6. Tuning the top surface affinity for each BCP component when the sidewall attracts component A produced four distinct morphologies: (red square) vertical orientation with minimal to no defects and a thin layer over the top surface; (blue square) vertical orientation with minimal to no defects without this thin layer; (red circle) vertical orientation with defects and a thin layer; (blue circle) vertical orientation with defects without a thin layer. $W = 8.13\ R_g$ ($2.0\ L_o$), $H = 4.06\ R_g$ ($1.0\ L_o$), taper is 68.2°, and $\Lambda_{SW}^{A} = 4.0$ and $\Lambda_{SW}^{B} = 6.0$.

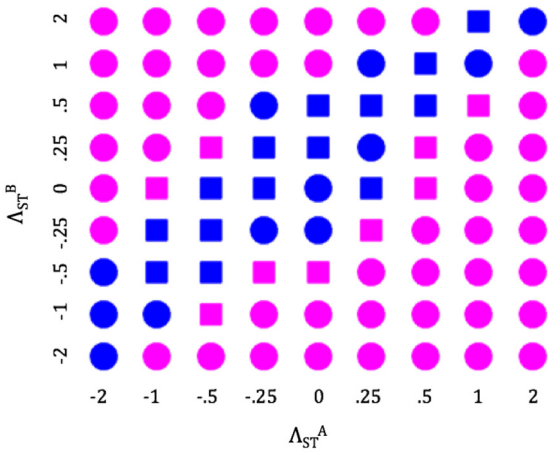

FIG. 8. Tuning the top surface affinity for each BCP component when the sidewall attracts component B produced four distinct morphologies: (red square) vertical orientation with minimal to no defects and a thin layer over the top surface; (blue square) vertical orientation with minimal to no defects without this thin layer; (red circle) vertical orientation with defects and a thin layer; (blue circle) vertical orientation with defects without a thin layer. $W = 8.13\ R_g$ ($2.0\ L_o$), $H = 4.06\ R_g$ ($1.0\ L_o$), taper is 68.2°, and $\Lambda_{SW}^{A} = 0.75$ and $\Lambda_{SW}^{B} = 0.5$.

distinct blocks of the BCP. A range of film-top interaction affinities (Λ_{FT}^{i}) were tested for perpendicular orientation conditions, and the optimum range was found to be when Λ_{FT}^{i} lies between 1.7 and 2.2. Subsequently, a series of parameter scans were undertaken simulations to determine the optimal interaction strengths of the sidewall to facilitate perpendicular orientation of the lamellae. Based on such results, the optimal range of sidewall chemical interaction strengths (Λ_{SW}) for favorable orientation was found to be 0.4 and 1.0, and Λ_{SW}^{A} was set at 0.75 and Λ_{SW}^{B} at 0.5, so that the sidewall attracts component B. Figures 7(c) and 7(d) display representative snapshots portraying the influence of $|\Lambda_{ST}^{A} - \Lambda_{ST}^{B}|$. Similar to the results discussed when the top and sidewall are attracted to the same component, Fig. 8 reveals that when the difference between Λ_{ST}^{A} and Λ_{ST}^{B} is large [Fig. 7(c)], a film of the preferential component is formed on top of the guideline. In general, less defective perpendicular orientation of lamellae was found to be facilitated when there exists only a small disparity between Λ_{ST}^{A} and Λ_{ST}^{B} [Fig. 7(d)]. Based on such results, the set of interaction parameter values chosen for the results presented in Sec. IV C were $\Lambda_{FT}^{A} = \Lambda_{FT}^{B} = 2.1$, $\Lambda_{ST}^{A} = 0.0$, $\Lambda_{ST}^{B} = 0.25$, $\Lambda_{SW}^{A} = 0.75$, $\Lambda_{SW}^{B} = 0.5$.

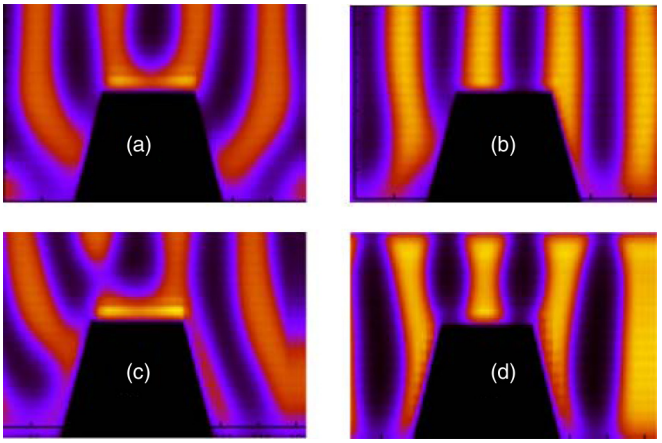

FIG. 7. 2D density profiles. (a), (b) Sidewall and top surface of the guideline attract the same component; (c), (d) Sidewall and top surface of the guideline attract different components; Strong disparity between Λ_{ST}^{A} and Λ_{ST}^{B} for (a) and (c); and weak disparity between Λ_{ST}^{A} and Λ_{ST}^{B} for (b) and (d). $\{\Lambda_{ST}^{A}, \Lambda_{ST}^{B}\}$ = (a) $\{-3,2\}$; (b) $\{-1,-2\}$; (c) $\{1,-1\}$; (d) $\{-0.5,-0.25\}$.

B. Sidewall and top surfaces exhibiting preferences for same components

In this section, we present results corresponding to the situation where both the sidewall and the top of the guideline surface were considered to be preferential to the same component. For such cases, lamellae orientation and alignment is expected to be optimal when the width of the top of the guideline (W_{top}) is commensurate with the lamellar domain spacing, *i.e.*, $W_{top} = nL_0$, where n is a positive integer.

1. Influence of χN

With the choices for the interaction parameters discussed in the Sec. IV A, we undertook a parametric scan of the influence of χN on the scores achieved in perpendicular orientation. The results of such studies, displayed in Fig. 9(a) [2D density map representation of the corresponding scores are provided in Fig. 9(b)], indicate that for stronger extent of segregation (higher χN), larger guideline widths are necessary to overcome the competing energetics. Moreover, the scores are in general seen to be lower for larger χN, due to the prevalence of metastable, defective morphologies. More explicitly, the

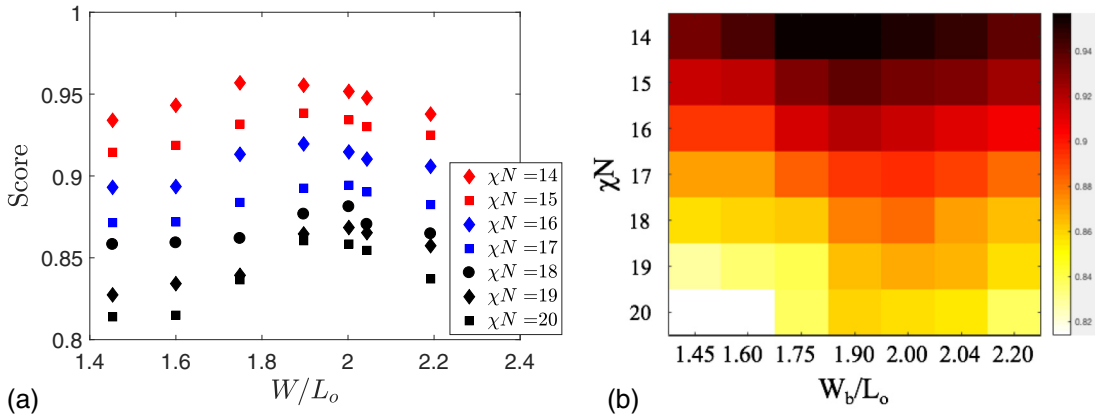

FIG. 9. (a) Effect of χN and guideline width on vertical lamellar formation when the top surface and sidewall attract the same blocks of the BCP; (b) 2D color map depiction for scores as a function of χN for $H = L_o$ and taper angle $\theta = 68.2^\circ$.

results in Fig. 9 indicate that χN in the range between 14.0 and 16.0 constitutes the optimal range for less defective lamellar formation. Based on such findings, and guided by the typical experimental conditions [22,23], for the results discussed in the following section, we fixed $\chi N = 14$.

2. *Influence of guideline geometry*

Figure 10(a) displays the scores for the perpendicular morphologies when the taper angle and the bottom widths of the guidelines are varied while their height is fixed. For clarity, a 2D density map representation of the corresponding scores are also provided in Fig. 10(b). Explicitly, the taper angle was varied in the range between 58.2° (a near triangular guideline)—90° (rectangular) and the effect on the orientation of the lamella was probed. Two general trends are seen to emerge from the results displayed:

(i) Independent of the guideline width, the optimal scores are observed for the case of intermediate taper angle guidelines (corresponding to a guideline angle of ≈70°);

(ii) Across the range of guideline taper angles, there is seen to exist an optimal, intermediate width which promotes the formation of perpendicular orientations (manifesting around $W/L_0 \approx 1.9$).

To rationalize the result (i) above, we note that rectangular and near rectangular guidelines ($\theta \gtrsim 80^\circ$) manifest a larger degree of constraints for the assembly of the BCPs. Indeed, on the one hand, guidelines with a steeper sidewall impose more stringent constraints on the geometry of the guideline to match the energetic preferences of the different components arising in the lamellar assembly. Moreover, steeper guidelines possess a smaller surface area for the sidewalls (relative to more tapered guidelines) and hence exert less of an energetic influence from the favorable interactions with the A component. Such a situation is schematically depicted in Fig. 11(a) where it can be seen that the favorable sidewall interactions impact only the Region 1 of the A portion of the lamella, and omits the Region 2. Finally, for steeper guidelines, the region between the sidewall and the grafted brush layer on the substrate also presents a more conformationally restrictive region of space for the block copolymer segments (Fig. 12). Together, such features underlie the observation of more orientational defects for near rectangular guidelines when compared to more gradually tapered guidelines.

Interestingly, we observe that there is an optimal angle for the guideline taper beyond which the propensity for orientational defects increases. To explain such results, we observe that the top surface of guidelines which resemble

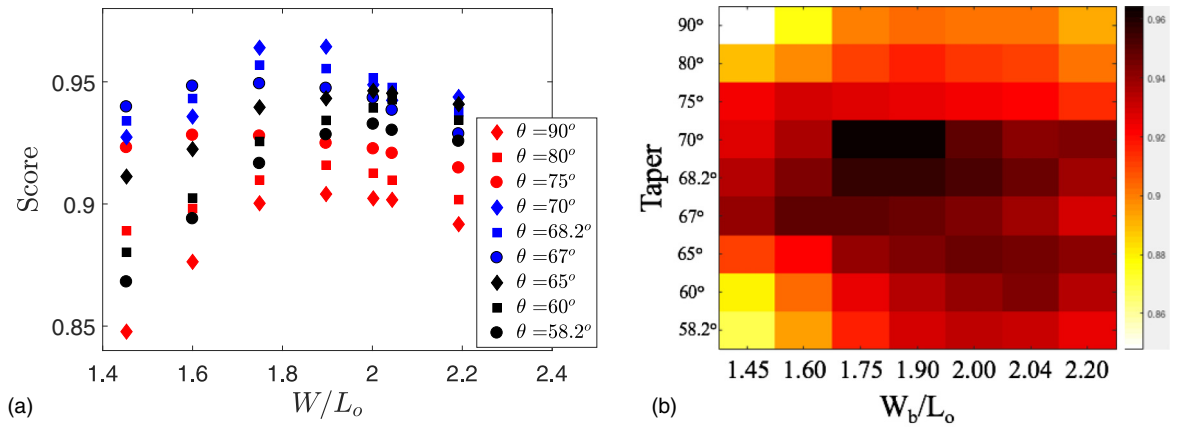

FIG. 10. (a) Effect of taper angle and guideline width on vertical lamellar formation when the top surface and sidewall attract the same component, with $H = L_0$; (b) 2D color maps for scores as a function of taper angle.

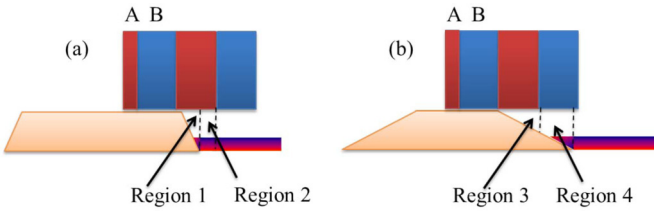

FIG. 11. Schematic representation of the competing energetics for the case where A segments are attracted by both top and by side (for clarity, only half planes for the lamellae are shown in the figures). (a) Steep taper: Due to steeper incline, A segments in Region 2 are unable to take advantage of the favorable interactions with the sidewalls of the guidelines; (b) Shallow taper: Shallow taper exposes the side wall area to the B segments in Region 4.

triangular topology do not present sufficient driving force for alignment of the lamella. Moreover, in such cases, the width of the guideline side wall also becomes larger than $0.5L_0$ resulting in an energetic penalty arising from the contact of B segments (Region 4) with the side walls [Fig. 11(b)].

The influence of the width of the guidelines [result (ii) above] can be rationalized similarly by invoking the unfavorable energetic interactions arising in the situations where guideline widths are either too small or too large. In the former situation, the lamellar morphologies cannot simultaneously take advantage of the favorable energetic interactions between the top and side surfaces of the guidelines and the A segments [Region 2 in Fig. 13(a)]. On the other hand, widths which are too large suffers from the unfavorable energetic interactions

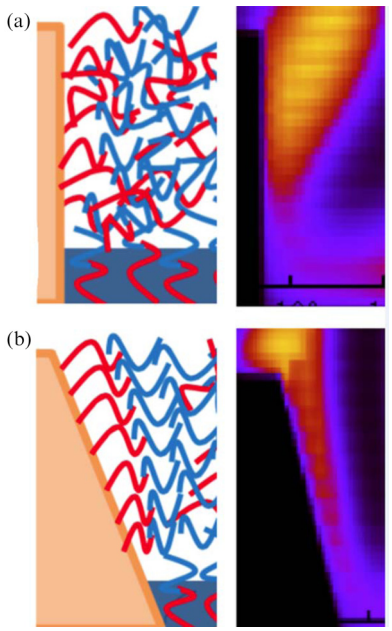

FIG. 12. Schematic representations of chain conformations and the resulting density maps. (a) Steep taper: Due to the presence of steep taper there is less area available for conformational rearrangement of random copolymer brush and the overlaying polymer segments; (b) Intermediate taper: An inclined sidewall is seen to present more conformational freedom for the brush and the overlaying polymer.

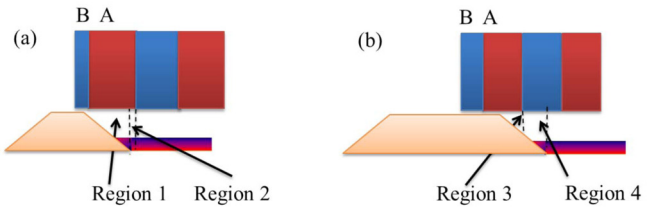

FIG. 13. Schematic representation of the competing energetics for the case where A segments are attracted by both top and by side (for clarity, only half planes for the lamellae are shown in the figures). (a) Smaller bottom width: Due to smaller widths, A segments in Region 2 are unable to take advantage of the favorable interactions with the sidewalls of the guidelines; (b) Large bottom width: Larger bottom width exposes the side wall area to the B segments in Region 4.

arising as a consequence of the contact of B segments with the side walls [Fig. 13(b)].

Overall, the above results are seen to suggest that guidelines with steeper taper angle are more susceptible to defects in vertical orientation, and more pertinently, the observation that rectangular guidelines typically envisioned for DSA processes may not be the most efficient geometry for guided self-assembly into perpendicular lamellar domains. Rather, intermediate tapers are seen to lead to higher favorability across all guideline widths.

In Fig. 14, we report the results for the influence of the guideline height on the lamellar orientation for two cases, corresponding respectively to intermediate (68.2°) and steep (80°) taper guideline angles. Similar to previous cases, 2D density map representation of the corresponding scores are provided in Figs. 14(c) and 14(d) for intermediate (68.2°) and steep (80°) taper guideline angles, respectively. For both situations, less defective perpendicular morphologies are seen to occur when the guideline height is in the range between $3R_g$ and $4R_g$. Consistent with the discussion above, we observe that the scores are in general lower for guidelines possessing steeper taper angles, and that there exists an optimal guideline width for achieving perpendicular morphologies.

To rationalize the influence of the guideline height, we note that guidelines with short heights [Fig. 15(a)] possess side walls with smaller surface areas, and hence exert a weaker energetic influence on the lamellar assemblies. On the other hand, tapered (nonrectangular) guidelines possessing large heights [Fig. 15(b)] are expected to lead to energetically unfavorable situation arising from small top surfaces of the guidelines and the accompanying contact between the B segments and the sidewalls. As a consequence, an optimal guideline height is expected to occur at intermediate conditions wherein the A segments of the lamella can fully take advantage of the favorable interactions with both top surface the side walls of the guidelines.

C. Sidewall and top surfaces exhibiting preferences for different components

In the results described in the previous section, the top surface and the sidewalls of the guideline were modeled as being preferential to the same component ($\Lambda^A_{SW} < \Lambda^B_{SW}$ and

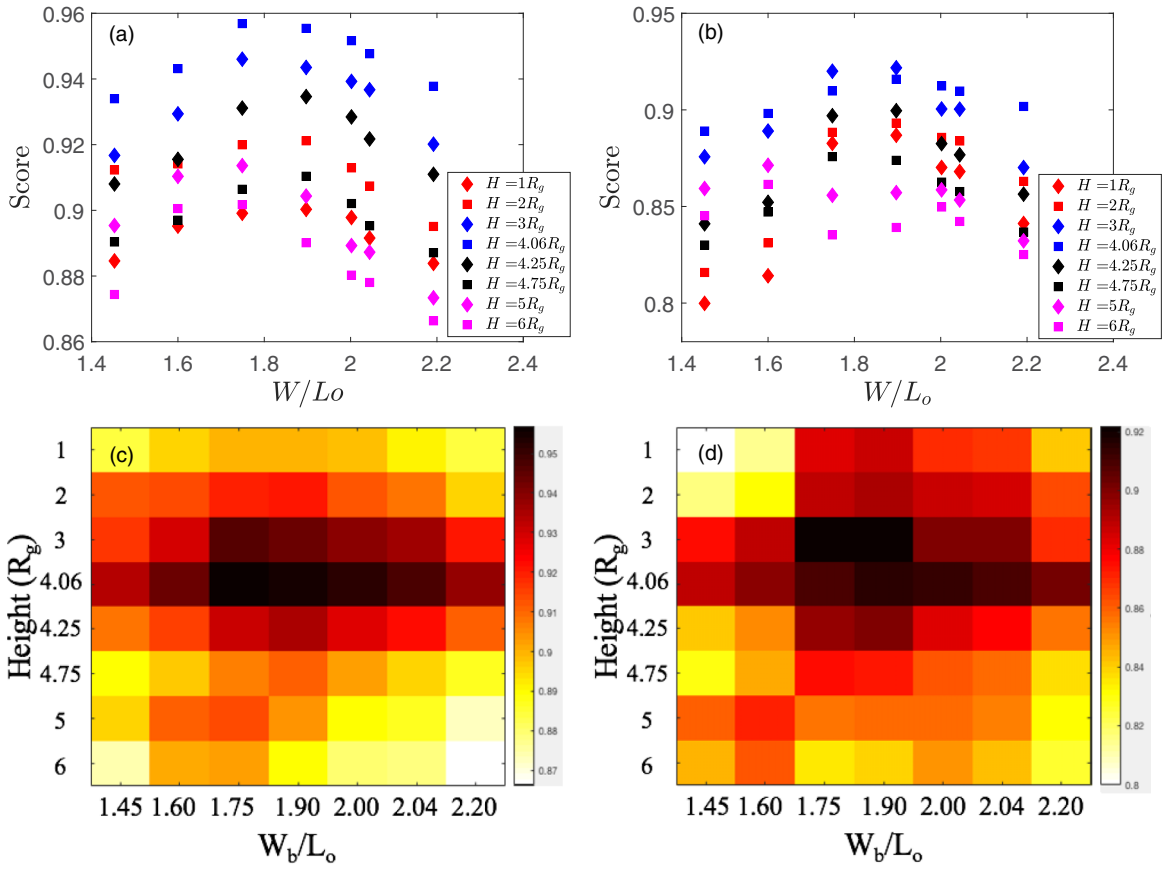

FIG. 14. Morphological scores as a function of the variation in guideline width for different guideline heights at taper angle corresponding to (a) 68.2° (left); and 80° (right). 2D color maps for scores as a function of (c) Height with 68° taper angle and; (d) Height with 80° taper angle.

$\Lambda^A_{ST} < \Lambda^B_{ST}$). In the present section, we present results for the influence of the guideline geometry for the situation in which the top surface is preferential to component A, whereas the sidewall is preferential to component B. In Sec. IV A we discussed the studies underlying the choice of various energetic parameters for such a case. In addition, similar to the results presented in the Sec. IV B 1, we undertook a parametric scan of the influence of the interaction parameter χ, and found that less defective perpendicular morphologies were found to occur for χN in the range between 14.0 and 16.0, as revealed in Fig. 16(a) and its corresponding color map in Fig. 16(b). For the results described in the following sections, we adopted $\chi N = 14.0$.

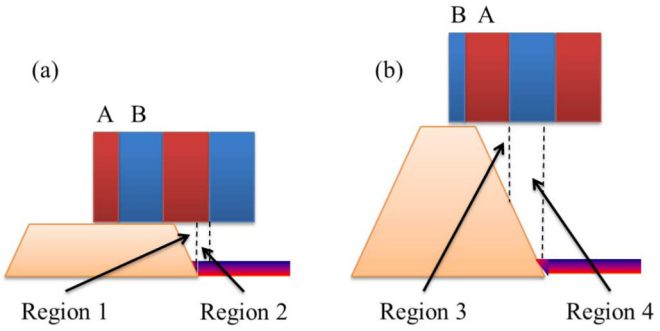

FIG. 15. Schematic representation of the competing energetics for the case where A segments are attracted by both top and by side (for clarity, only half planes for the lamellae are shown in the figures). (a) Small heights: Due to smaller heights, A segments in Region 2 are unable to take advantage of the favorable interactions with the sidewalls of the guidelines; (b) Large heights: Larger height exposes the side wall area to the B segments in Region 4.

For cases where the sidewall and top surfaces exhibit preferences to different components, perpendicularly oriented lamellae are expected to be favored when the width of the *top of the guideline*: $W_{top} = (2n-1)L_0/2$, where n is an integer. In such a case, the B segments can take advantage of the favorable energetics offered by the side walls while the A segments assemble on the (favorable) top wall of the guidelines. However, such simplistic considerations do not account for the possible adaptation of the morphologies themselves in response to the guideline width, taper angle, and heights. In the following sections, we present results quantifying the influence of such geometric features on the defects resulting in perpendicular morphologies.

1. *Influence of guideline geometry*

Figure 17(a) displays the results for the orientational defects of morphologies resulting when the taper angle of the guideline was modulated. Corresponding color maps are provided in Fig. 17(b). Similar to the results discussed in

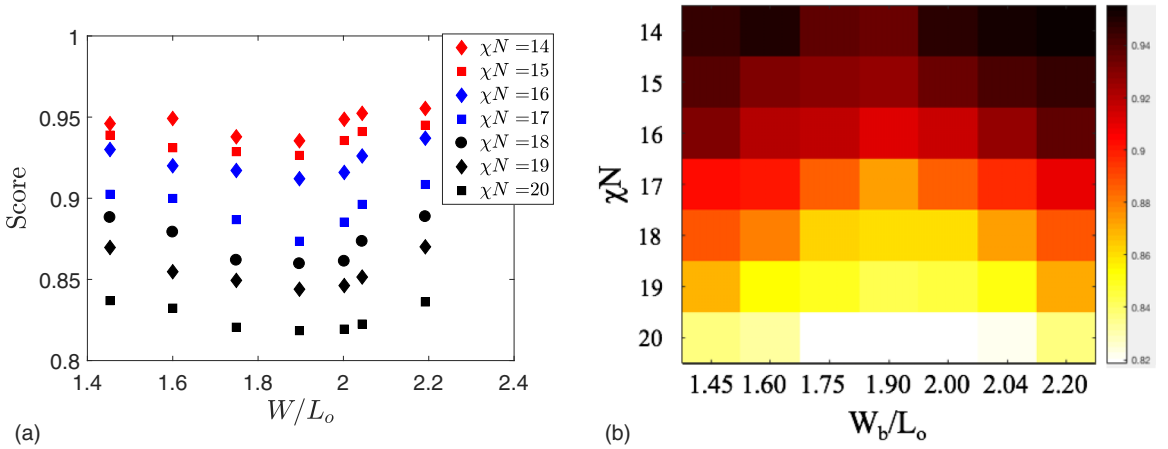

FIG. 16. Effect of χN and guideline width on vertical lamellar formation when the top surface and sidewall attract different components with $H = 4.06\ R_g$ and taper angle to 68.2° using (a) normal plot; (b) 2D representation.

Sec. IV B 2, intermediate taper angles (67°, 68.2°, 70°) are observed to result in favorable conditions for perpendicular lamella (scores greater than 0.92) across all guideline widths. Pertinently, we again observe that the rectangular guideline with a 90° taper is seen to possess the lowest score for nearly all guideline widths. In contrast to the results obtained for the case wherein the substrate top and sidewall attracted the same component (which showed a maximum around $W/L_0 = 1.9$ across all taper angles), for the present case, we observe that for intermediate taper angles (≈67–70°), the scores decrease slightly at intermediate widths. However, for the case of large tapering angles (>80°), the scores are indeed seen to become smaller with increasing guideline bottom widths.

To rationalize the taper angle dependence observed in Fig. 17, we again invoke the explanation proposed in the Sec. IV B 2. Explicitly, smaller taper angles (corresponding to near triangular guidelines) result in larger widths for the sidewalls and smaller widths for the top of the guidelines, and is expected to lead to energetically unfavorable interactions between the A segments of the copolymer and the sidewalls [Region 2 in Fig. 18(a)]. In contrast, larger taper angles (near rectangular guidelines) are expected to lead to more constraints on the block copolymer assembly, arising from both the need to ensure that lamella are geometrically commensurate with the guideline widths, and the conformational constraints imposed by steeper guidelines. The former factor is seen most manifestly in the results for rectangular guidelines (Fig. 17), in which changes in the guideline widths are seen to result in a sharp decrease in the scores. Further, steeper guidelines also lead to smaller surface areas for the sidewalls (relative to tapered guidelines) and thereby exert less of a favorable energetic influence on the B segments [Fig. 18(b)].

Figures 19(a) and 19(b) display results arising from the modulation of guideline heights for taper angles fixed at 68.2° (shallow) and 80° (steep), respectively [(2D density map representation of the corresponding scores are provided in Figs. 19(c) and 19(d)]. The qualitative features exhibited by such results are seen to match with those discussed in the context of Fig. 17. Explicitly, for intermediate tapers [Fig. 19(a)], intermediate widths result in a drop in scores, and for steeper taper angles [Fig. 19(b)], changes in guideline widths are seen to lead to a significant drop in the scores.

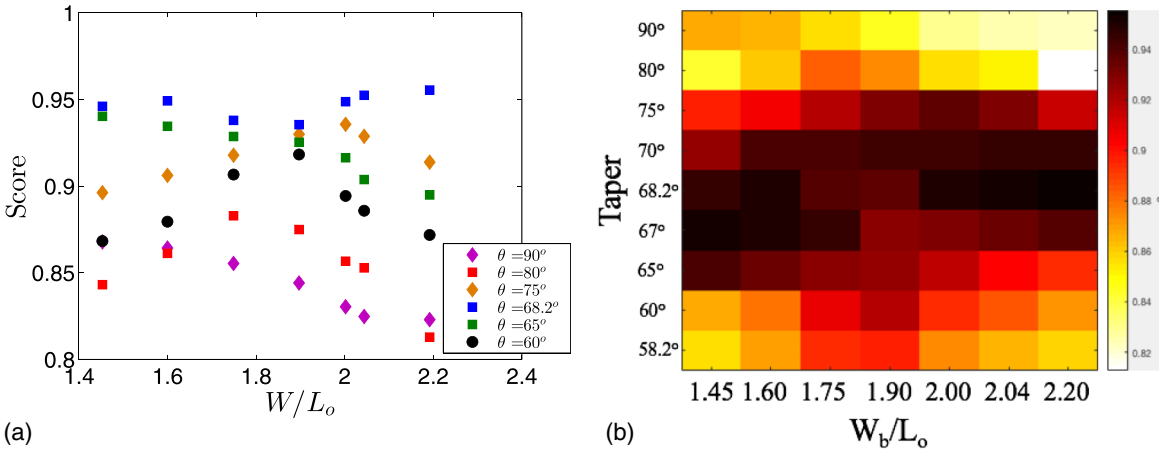

FIG. 17. Effect of taper angle and guideline width on vertical lamellar formation when the top surface and sidewall are attracted to different components, with $H = 4.06\ R_g$ using (a) 2D plot; (b) 2D color map.

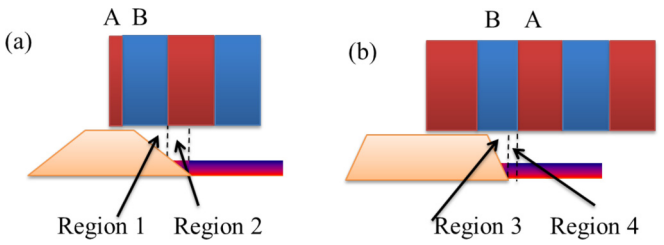

FIG. 18. Schematic representation of the competing energetics for the case where A segments are attracted by both top and B segments are attracted by the sidewall (for clarity, only half planes for the lamellae are shown in the figures). (a) Shallow taper: Shallow taper exposes the side wall area to the A segments in Region 2; (b) Steep taper: Due to steeper incline, B segments in Region 4 are unable to take advantage of the favorable interactions with the sidewalls of the guidelines.

The influence of guideline heights are seen to be similar to those discussed in Sec. IV B 2 in the context of Fig. 14. Explicitly, less defective perpendicular morphologies are seen to occur when the guideline height is roughly between $3R_g$ and $4R_g$. Such results can be rationalized by noting that side walls of guidelines possessing short heights are expected to exert a weaker energetic influence on the assembly due to the smaller surface areas of the side walls. On the other hand, guidelines possessing large heights are expected to lead to the energetically unfavorable situation arising from contact between the A segments of the BCP and the sidewalls. Hence, intermediate guideline heights occurring at conditions for which the B segments of the lamella can fully take advantage of the favorable interactions with the side walls are expected to be optimal.

D. Best structures

In this section, we present the best score scenario for the cases for (a) surface and sidewall attracting the same component and; (b) surface and sidewall attracting different components. In Fig. 20(a), we display the equilibrium lamellar structure with the highest score when the top surface and sidewall attracted the same component. The computed score for such a case is 0.964. Further, the parametric conditions for such a case correspond to $H = 4.06R_g$, $W = 1.75L_o$, and $\theta = 70^\circ$. In Fig. 20(b), we display the lamellar structure with the highest score when the the top surface and sidewall attracted different components, and the computed score is 0.955. The parametric conditions for such a case correspond to $H = 4.06R_g$, $W = 2.19L_o$, and $\theta = 68.2^\circ$. In both the cases, it can be seen that the maximum score is obtained at intermediate taper angles.

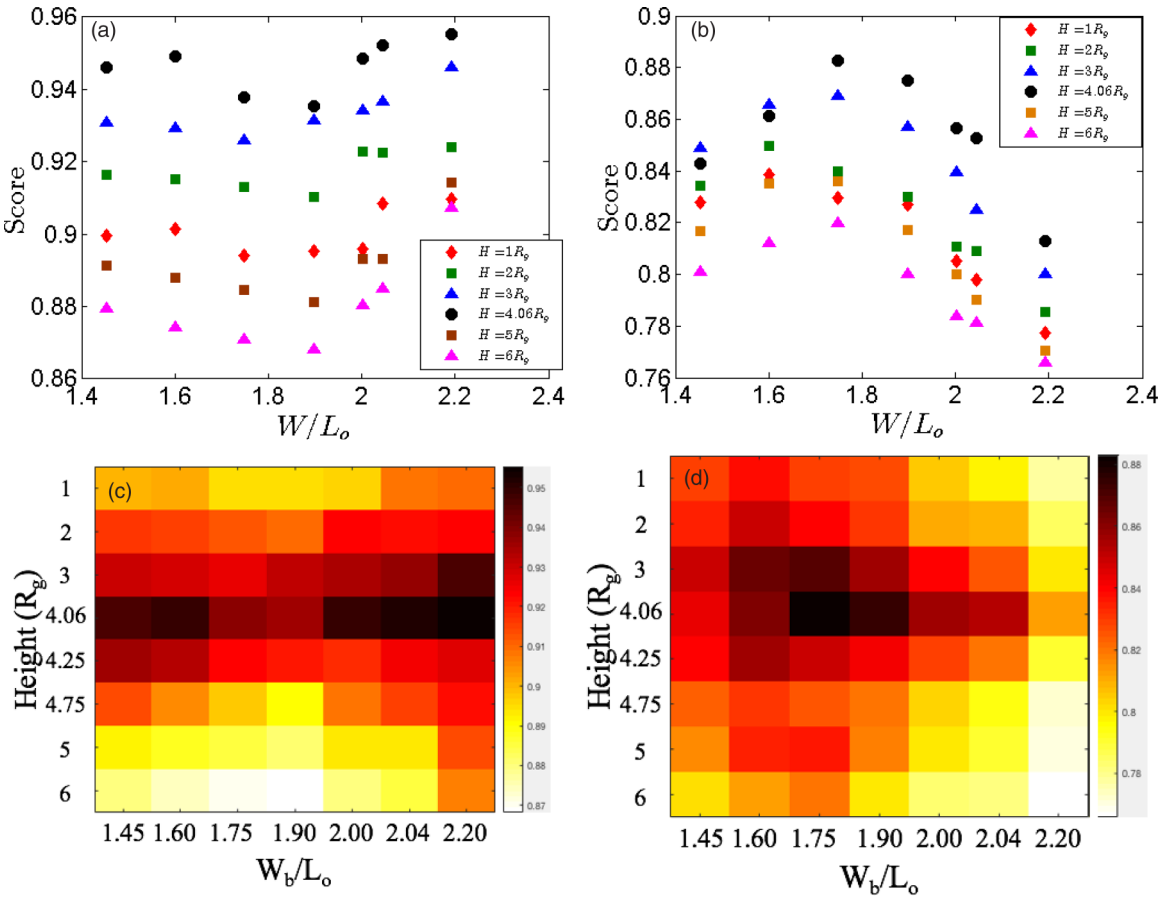

FIG. 19. Variation of guideline height (H) versus width (W) at (a)/(c) 68.2° (left) and; (b)/(d) 80° (right) when the top surface and sidewall attract different components.

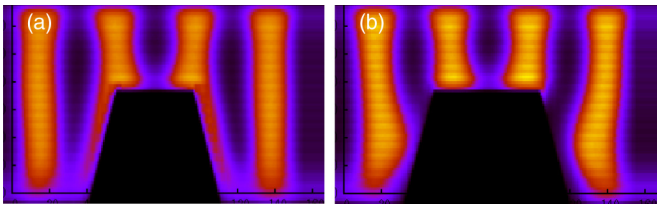

FIG. 20. Best lamellar structure (highest score) for (a) when surface and sidewall attract same component; (b) when surface and sidewall attract different components.

V. CONCLUSIONS

In summary, the methodology of single chain in mean-field simulations was adopted to study the self-assembly of block copolymers in thin films with trapezoidal guidelines to probe the influence of the geometry of the guidelines on the formation of perpendicularly oriented lamellar orientations. Our results were quantified in terms of normalized scores with respect to the ideal, perpendicularly oriented lamella. We considered two situations: (i) The guideline top and sidewall exhibits preferential interactions with the same component of the block copolymer; and (ii) The guideline top and sidewall exhibits preferential interactions with different components of the block copolymer.

For both cases above, our results suggest that guidelines with tapered walls are more efficacious relative to rectangular geometries in promoting defect free, perpendicularly oriented lamella. However, an optimal tapering angle was found, beyond which trapezoidal guidelines became less effective. Similarly, optimal values were found for the guideline widths and heights which promoted less defective perpendicularly oriented lamella. Such observations were rationalized by invoking (mainly) considerations arising from the energetics of the interaction of the side walls with the two components of the block copolymer. Together, our results suggest that careful tuning of the guideline geometries can serve a versatile parametric handle to guide the orientation (and alignment) of BCP morphologies for lithographic applications.

ACKNOWLEDGMENTS

This work was supported in part by a grant from Robert A. Welch Foundation (Grant No. F1599) and to the Donors of the American Chemical Society Petroleum Research Fund for partial support of this research (Grant No. 56715-ND9). The authors acknowledge the Texas Advanced Computing Center (TACC) at The University of Texas at Austin for providing computing resources that have contributed to the research results reported within this paper. G.B. thanks the Paul D. Meek Endowed Graduate Fellowship in Engineering for support.

[1] D. J. C. Herr, J. Mater. Res. **26**, 122 (2011).
[2] S. B. Darling, Prog. Polym. Sci. **32**, 1152 (2007).
[3] C. M. Bates, M. J. Maher, D. W. Janes, C. J. Ellison, and C. G. Willson, Macromolecules **47**, 2 (2014).
[4] S. H. Han, V. Pryamitsyn, D. Bae, J. Kwak, V. Ganesan, and J. K. Kim, ACS Nano **6**, 7966 (2012).
[5] R. Ruiz, E. Dobisz, and T. R. Albrecht, ACS Nano **5**, 79 (2011).
[6] H. Yi, X. Y. Bao, J. Zhang, C. Bencher, L. W. Chang, X. Chen, R. Tiberio, J. Conway, H. Dai, Y. Chen, S. Mitra, and H. S. P. Wong, Adv. Mater. **24**, 3107 (2012).
[7] T. R. Albrecht, D. Bedau, E. Dobisz, H. Gao, M. Grobis, O. Hellwig, D. Kercher, J. Lille, E. Marinero, K. Patel, R. Ruiz, M. E. Schabes, L. Wan, D. Weller, and T.-W. Wu, IEEE Trans. Magn. **49**, 773 (2013).
[8] B. D. Terris, J. Magn. Magn. Mater. **321**, 512 (2009).
[9] T. Seshimo, R. Maeda, R. Odashima, Y. Takenaka, D. Kawana, K. Ohmori, and T. Hayakwa, Sci. Rep. **6**, 19481 (2016).
[10] T. Lo, A. Dehghan, P. Georgopanos, A. Avgeropoulos, A. C. Shi, and R. M. Ho, Macromolecules **49**, 624 (2016).
[11] X. M. Yang, R. D. Peters, P. F. Nealey, H. H. Solak, and F. Cerrina, Macromolecules **33**, 9575 (2000).
[12] R. Ruiz, H. Kang, F. A. Detcheverry, E. Dobisz, D. S. Kercher, T. R. Albrecht, J. J. de Pablo, and P. F. Nealey, Science **321**, 936 (2008).
[13] S. O. Kim, H. H. Solak, M. P. Stoykovich, N. J. Ferrier, J. J. de Pablo, and P. F. Nealey, Nature **424**, 411 (2003).
[14] M. P. Stoykovich, H. Kang, K. C. Daoulas, G. Liu, C. C. Liu, J. J. de Pablo, M. Müller, and P. F. Nealey, ACS Nano **1**, 168 (2007).
[15] A. Ramírez-Hernández, G. Liu, P. F. Nealey, and J. J. de Pablo, Macromolecules **45**, 2588 (2012).
[16] P. Mansky, Y. Liu, E. Huang, T. P. Russell, and C. J. Hawker, Science **275**, 1458 (1997).
[17] E. Huang, T. P. Russell, C. Harrison, P. M. Chaikin, R. A. Register, C. J. Hawker, and J. Mays, Macromolecules **31**, 7641 (1998).
[18] C. C. Liu, A. Ramírez-Hernández, E. Han, G. S. W. Craig, Y. Tada, H. Yoshida, H. Kang, S. Ji, P. Gopalan, J. J. de Pablo, and P. F. Nealey, Macromolecules **46**, 1415 (2013).
[19] J. Cushen, L. Wan, G. Blachut, M. Maher, T. Albrecht, C. J. Ellison, C. G. Willson, and R. Ruiz, Appl. Mater. Interfaces **7**, 13476 (2015).
[20] G. Pandav, W. Durand, C. J. Ellison, C. G. Willson, and V. Ganesan, Soft Matter **11**, 9107 (2015).
[21] F. A. Detcheverry, G. Liu, P. F. Nealey, and J. J. de Pablo, Macromolecules **43**, 3446 (2010).
[22] G. Blachut, S. Sirard, M. Maher, Y. Asano, Y. Someya, A. Lane, W. Durand, C. Bates, A. Dinhobl, R. Gronheid, D. Hymes, C. J. Ellison, and C. G. Willson, Chem. Mater. **28**, 8951 (2016).
[23] L. D. Williamson, R. N. Seidel, X. Chen, H. Seon Suh, R. P. Delgadillo, G. Roel, and P. F. Nealey, ACS Appl. Mater. Interfaces **8**, 2704 (2016).
[24] M. Muller and G. D. Smith, J. Polym. Sci., Part B: Polym. Phys. **43**, 934 (2005).
[25] K. C. Daoulas, M. Muller, J. J. de Pablo, P. F. Nealey, and G. D. Smith, Soft Matter **2**, 573 (2006).
[26] K. C. Daoulas, M. Muller, M. P. Stoykovich, H. Kang, J. J. de Pablo, and P. F. Nealey, Langmuir **24**, 1284 (2008).
[27] J. Wang and M. Muller, Macromolecules **42**, 2251 (2009).
[28] J. Wang and M. Muller, J. Phys. Chem. B **113**, 11384 (2009).
[29] K. C. Daoulas and M. Muller, J. Chem. Phys. **125**, 184904 (2006).

[30] V. Ganesan and V. Pryamitsyn, J. Chem Phys. **118**, 4345 (2003).
[31] V. Ganesan and V. Pryamitsyn, J. Chem Phys. **136**, 101101 (2012).
[32] G. H. Fredrickson, *The Equilibrium Theory of Inhomogeneous Polymers* (Oxford University Press, Oxford, 2006).
[33] F. A. Detcheverry, P. F. Nealey, and J. J. de Pablo, Macromolecules **43**, 6495 (2010).
[34] G. Liu, F. Detcheverry, A. Ramírez-Hernandez, H. Yoshida, Y. Tada, J. J. de Pablo, and P. F. Nealey, Macromolecules **45**, 3986 (2012).
[35] A. Ramírez-Hernández, H. S. Suh, P. F. Nealey, and J. J. de Pablo, Macromolecules **47**, 3520 (2014).
[36] K. Binder and W. Paul, J. Polym. Sci., Part B: Polym. Phys. **35**, 1 (1997).
[37] V. Ganesan and H. Brenner, Phys. Rev. Lett. **81**, 578 (1998).
[38] T. Segal-Peretz, J. Ren, S. Xiong, G. Khaira, A. Bowen, L. E. Ocola, R. Divan, M. Doxastakis, N. J. Ferrier, J. J. de Pablo, and P. F. Nealey, ACS Nano **11**, 1307 (2017).
[39] W. Lee, S. Park, H. Lee, V. Sethuraman, N. Rebello, V. Ganesan, and D. Y. Ryu, Macromolecules **50**, 5858 (2017).